AGU PUBLICATIONS

Water Resources Research

RESEARCH ARTICLE
10.1002/2016WR019733

This article is a companion to *Baronas et al.* [2017], doi:10.1002/2016WR019729.

Special Section:
Concentration-discharge Relations in the Critical Zone

Key Points:
- Tributary mixing modulates concentration-discharge relationships
- Effect of tributary mixing varies between solutes
- Changes in tributary contributions are due to spatiotemporal precipitation patterns

Supporting Information:
- Supporting Information S1
- Data Set S1
- Data Set S2

Correspondence to:
M. A. Torres,
mtorres@caltech.edu

Citation:
Torres, M. A., J. J. Baronas, K. E. Clark, S. J. Feakins, and A. J. West (2017), Mixing as a driver of temporal variations in river hydrochemistry: 1. Insights from conservative tracers in the Andes-Amazon transition, *Water Resour. Res.*, *53*, 3102–3119, doi:10.1002/2016WR019733.

Received 31 AUG 2016
Accepted 22 FEB 2017
Accepted article online 17 MAR 2017
Published online 17 APR 2017

Mixing as a driver of temporal variations in river hydrochemistry: 1. Insights from conservative tracers in the Andes-Amazon transition

Mark A. Torres[1,2], J. Jotautas Baronas[2], Kathryn E. Clark[3], Sarah J. Feakins[2], and A. Joshua West[2]

[1]Division of Geology and Planetary Sciences, California Institute of Technology, Pasadena, California, USA, [2]Department of Earth Sciences, University of Southern California, Los Angeles, California, USA, [3]Department of Earth and Environmental Sciences, University of Pennsylvania, Philadelphia, Pennsylvania, USA

Abstract The response of hillslope processes to changes in precipitation may drive the observed changes in the solute geochemistry of rivers with discharge. This conjecture is most robust when variations in the key environmental factors that affect hillslope processes (e.g., lithology, erosion rate, and climate) are minimal across a river's catchment area. For rivers with heterogenous catchments, temporal variations in the relative contributions of different tributary subcatchments may modulate variations in solute geochemistry with runoff. In the absence of a dense network of hydrologic gauging stations, alternative approaches are required to distinguish between the different drivers of temporal variability in river solute concentrations. In this contribution, we apportion the water and solute fluxes of a reach of the Madre de Dios River (Peru) between its four major tributary subcatchments during two sampling campaigns (wet and dry seasons) using spatial variations in conservative tracers. Guided by the results of a mixing model, we identify temporal variations in solute concentrations of the main stem Madre de Dios that are due to changes in the relative contributions of each tributary. Our results suggest that variations in tributary mixing are, in part, responsible for the observed concentration-discharge (C-Q) relationships. The implications of these results are further explored by reanalyzing previously published C-Q data from this region, developing a theoretical model of tributary mixing, and, in a companion paper, comparing the C-Q behavior of a suite of major and trace elements in the Madre de Dios River system.

1. Introduction

Rivers are thought to integrate biogeochemical processes across their catchment area and contribute significantly to the fluxes of water and solutes delivered to the ocean [*Gaillardet et al.*, 1999]. Due to their size and the heterogeneity of their catchment area, it can be difficult to derive mechanistic models of hydrology and solute geochemistry from the study of larger rivers. Consequently, many researchers have focused on understanding the hydrochemistry of hillslopes and small homogeneous catchments as the basis for developing process-based models [e.g., *Anderson et al.*, 1997; *Stallard and Murphy*, 2014; *Kim et al.*, 2014; *Herndon et al.*, 2015]. An outstanding question is how to appropriately scale models based on hillslopes and small catchments in order to describe the behavior of larger river systems, and what spatial scale begins to introduce heterogeneity that may complicate interpretation of hydrochemical signatures.

Temporal variations in the solute geochemistry of rivers are often correlated with changes in water discharge [*Johnson et al.*, 1969; *Godsey et al.*, 2009; *Calmels et al.*, 2011; *Moon et al.*, 2014; *Moquet et al.*, 2015; *Torres et al.*, 2015]. A variety of different models have been developed in order to explain these concentration-discharge (C-Q) relationships, ranging from source mixing [*Johnson et al.*, 1969; *Calmels et al.*, 2011] to reactive-transport processes occurring within hillslopes [*Godsey et al.*, 2009; *Maher*, 2011; *Maher and Chamberlain*, 2014]. Since many of the hypothesized drivers of C-Q relationships are thought to depend upon environmental factors (e.g., lithology, erosion rate, and climate), C-Q relationships are expected and observed to vary spatially [*Godsey et al.*, 2009; *Moon et al.*, 2014; *Torres et al.*, 2015; *Ibarra et al.*, 2016]. As a result, many catchments can be considered to be composed of smaller tributary subcatchments that each have their own distinct C-Q relationships.

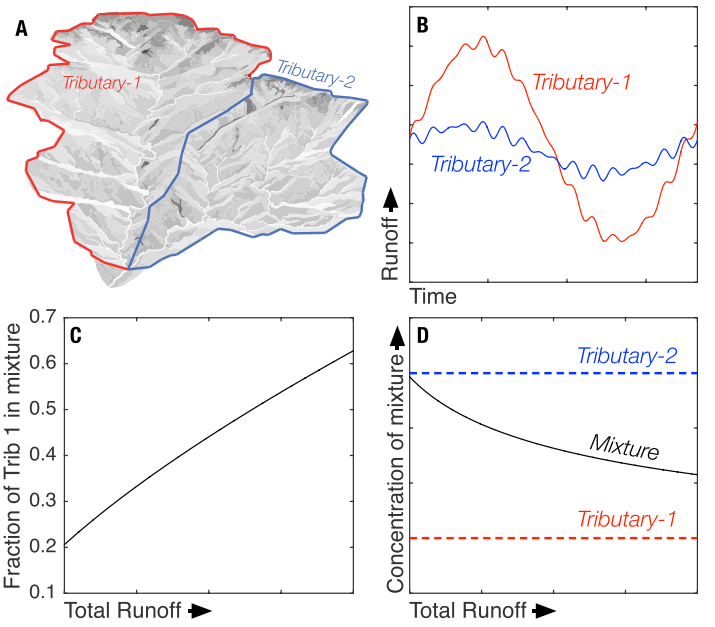

Figure 1. Tributary mixing schematic. (a) River catchment comprised of two tributary subcatchments. (b) Hypothetical runoff time series for the two catchments assuming that they receive different amounts of rainfall and/or have different rainfall-runoff relationships. (c) The relative contribution of tributary 1 to total discharge as implied by the time series in Figure 1b, which, crucially, varies with discharge. (d) We show how the mixing ratio shown in Figure 1c could lead to solute dilution with increasing runoff even if the two subcatchments had constant, but distinct, solute concentrations. Additional tributary mixing scenarios are shown in Figure 10.

The observed C-Q relationship of a river main stem reflects a flux-weighted average of its constituent subcatchments. A priori, the weighting function that describes the relative contribution of each tributary is unknown. The relative contribution from each tributary can vary temporally as a result of spatial variations in the timing and amount of precipitation and/or variations in rainfall-runoff relationships. The combination of spatially variable C-Q relationships and temporally variable tributary contributions can result in a different C-Q relationship of the main stem compared to its constituent subcatchments (see Figure 1 for a schematic illustration).

The importance of tributary mixing in determining C-Q relationships should depend upon the magnitude of spatial variability in runoff and solute generation. Since many of the factors that are thought to control solute and runoff generation (e.g., precipitation, lithology, morphology) are spatially correlated, it is reasonable to expect that the relative importance of heterogeneous tributary mixing will increase with increasing catchment area. Nevertheless, it is important to directly characterize whether or not there exists sufficient heterogeneity in large catchments to meaningfully impact C-Q relationships, and to consider at what catchment scale these effects become important. In this study, we seek to characterize whether the relative contributions of constituent tributaries to a large river system vary with discharge and whether the C-Q relationships of these tributaries are significantly different from each other.

Specifically, we explore tributary mixing in the Madre de Dios River system (catchment area $\approx 28 \times 10^3$ km^2), which drains the Peruvian Andes and Amazon. The large gradients in topography, rainfall, and lithology in this basin provide the kind of heterogeneity that we expect to make tributary mixing important in setting C-Q relationships. Our previous work on this system [*Torres et al.*, 2015] indicated that C-Q relationships vary systematically with catchment slope angle, a proxy for erosion rate, in a manner consistent with existing models for a hillslope-scale control on C-Q relationships [e.g., *Maher and Chamberlain*, 2014]. However, catchment area covaries with catchment slope angle in the *Torres et al.* [2015] study such that effects of heterogeneous tributary mixing may be superimposed on an underlying erosional control of C-Q relationships.

To apportion the water and solute budgets of the Madre de Dios River between its four main tributaries, we employ a mixing approach using conservative tracers, mostly relying on differences between the water isotopic composition of each tributary. Our results suggest that the relative contributions of different tributary subcatchments vary seasonally due to observed precipitation patterns, and that these differences modulate the C-Q relationships of the main stem. To better understand the implications of these results, we develop a simple forward model of tributary mixing as well as reanalyze data from an Andean headwater catchment reported in *Torres et al.* [2015] where the effects of tributary mixing on C-Q relationships can be distinguished for different elements even in a catchment with an area of ~160 km^2. Finally, in a companion paper *Baronas et al.* [2017], we explore the effects of tributary mixing on the C-Q behavior of a suite of 23 major and trace elements in the entire Madre de Dios River system.

2. Methods

2.1. Study Area

This study focuses on the Madre de Dios River, its major tributaries, and its headwaters in the Andean Kosñipata valley in Peru (Figure 2). Detailed information about the climatic conditions [*Espinoza et al*., 2015; *Feakins et al*., 2016], hydrology [*Clark et al*., 2014], and lithology [*Torres et al*., 2016] of this river system is available in previously published work. Briefly, the catchment is heterogeneous with respect to temperature (mean annual temperature between 5 and 25°C) [*Lambs et al*., 2012; *Feakins et al*., 2016] and precipitation (mean annual precipitation between 2 and 5 m yr^{-1}) [*Lambs et al*., 2012; *Feakins et al*., 2016] due to its the large elevation range (Figure 2). The headwaters of the catchment are underlain by Paleozoic sedimentary and metasedimentary rocks, Mesozoic sedimentary rocks, and minor igneous intrusions. Lower elevations are underlain by Paleogene to Holocene sediment deposits sourced from Andean erosion [*Mendívil Echevarría and Dávila Manrique*, 1994; *Carlotto Caillaux et al*., 1996; *Vargas Vilchez and Hipolito Romero*, 1998; *INGEMMET*, 2013].

Between 2010 and 2013, the Madre de Dios River was sampled for solute concentrations and water isotope ratios at the CICRA gauging station (Figure 2). Following *Torres et al*. [2016], we will refer to this catchment as the Foreland-floodplain site. The river gauging reported in *Torres et al*. [2015] ceased after 2010, but discharge at the Foreland-floodplain site was also measured during sampling campaigns in March and August 2013 using an Acoustic Doppler Current Profiler (RD1 Sentinel GED154 in March 2013 and SonTek M9 in August 2013).

For the purpose of investigating temporal variations in the relative contributions of different subcatchments to total water and solute fluxes, we divide the Foreland-floodplain catchment into its four major tributaries: the Alto Madre de Dios River (26% of total catchment area), the Manu River (46% of total catchment area), the Chiribi River (4% of total catchment area), and the Colorado River (12% of total catchment area; Figure 2). Together, these tributaries account for almost 90% of the catchment area of the Foreland-floodplain site. The Alto Madre de Dios and Manu Rivers have a majority of their catchment areas within the Andes Mountains (>400 m; 95 and 68%, respectively). In contrast, the Chiribi and Colorado Rivers have a majority of their catchment area within the foreland-floodplain (<400 m; 60 and 52%, respectively). The full catchment elevation

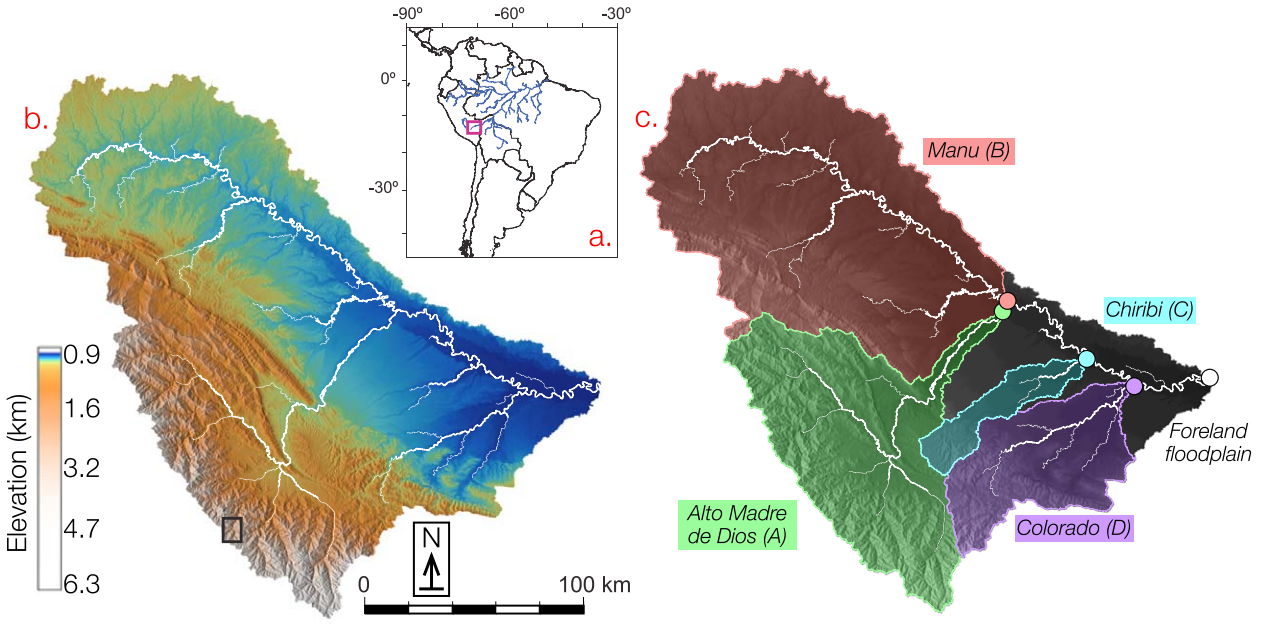

Figure 2. Study area. (a) The location of the study area within the larger Amazonian region. (b) Shaded relief/elevation map of the catchment area of the Madre de Dios River at the CICRA gauging station (Foreland-floodplain site). In (c), we divide the catchment area of the Madre de Dios River into its four major tributary subcatchments, which are labeled (A) through (D) depending upon their downstream position. In Figure 2b, the small box within high Andes Mountains is the approximate location of the Kosñipata River catchments (Wayqecha/Mountain-1 and San Pedro/Mountain-2 sampling stations) of *Torres et al*. [2015] and *Torres et al*. [2016].

distributions are shown in supporting information Figure S1. For simplicity, we will refer to each catchment as tributary-A (Alto Madre de Dios River), tributary-B (Manu River), tributary-C (Chiribi River), and tributary-D (Colorado River), which orders the catchments from upstream to downstream (Figure 2).

2.2. Sample Collection

River waters were sampled with a plastic container and filtered with a 0.2 μm porosity filter (either nylon or polyethylsulfone) in the field before storage in glass exetainers and/or high-density polyethylene (HDPE) bottles. All bottles and vials were filled completely with water so that samples were stored without significant headspace. For samples collected in both glass exetainers and HDPE bottles, no offset in the water isotope composition was observed between the different containers. Samples for cation analysis (collected into HDPE bottles) were acidified by adding either concentrated HCl or HNO_3 (final pH $\approx$2).

2.3. Analytical Methods

2.3.1. GIS Analysis

To determine elevation distributions and catchment areas, we used a digital elevation model (DEM) based on 3 arc second ($\sim$90 m) Shuttle Radar Tomography Mission (SRTM) data [*Jarvis et al.*, 2008]. To analyze spatiotemporal rainfall patterns, we used the Tropical Rainfall Monitoring Mission (TRMM) product 2B31 processed by B. Bookhagen (High resolution spatiotemporal distribution of rainfall seasonality and extreme events based on a 12-year trmm time series, in review) and available at http://geog.ucsb.edu/bodo/TRMM/. The 2B31 product is produced from precipitation radar and the TRMM microwave imager. It is a monthly product spanning from 1998 to 2007, at a resolution of 4 $\times$ 4 km. The analysis of both the DEM and TRMM data was completed using the GRASS GIS software package.

2.3.2. Water Isotopes

The stable H and O isotopic composition of river water was measured by laser spectroscopy using a Los Gatos Research DLT-1000 liquid water isotope analyzer at the California Institute of Technology as well as a Picarro Cavity Ring Down Spectrometer at the University of Southern California (USC). For both instruments, the first two injections were discarded in order to avoid memory effects, and measurements were determined for the subsequent six replicate injections at Caltech and three replicate injections at USC. Hydrogen and oxygen isotope ratios (as D:H and ^{18}O:^{16}O, respectively) are expressed in delta notation as "per mil" or parts per thousand (‰) relative to the Vienna Standard Mean Ocean Water (VSMOW)-Standard Light Antarctic Precipitation (SLAP) isotopic scale, with accuracy determined to better than 0.2‰ (δD) and 0.1‰ (δ^{18}O).

Replicate measurements yielded a mean precision (σ) of 0.6‰ for δD and 0.2‰ for $\delta^{18}O$ (n = 30) and were calibrated using three of four working standards run during each analytical session (Maui Water, δD = –10.6‰, $\delta^{18}O$=−3.3‰, Caltech internal standard, δD = −73.4‰, $\delta^{18}O$=−9.7‰, USC internal standard, δD = −60.5‰, $\delta^{18}O$=−8.2‰, and LGR Water #2, δD = −117.0‰ $\delta^{18}O$=−15.5‰). The internal standards (either USC or Caltech) were run every 15 samples during the course of each run. The same standards were run on both instruments in order to ensure comparability, which was validated by running a subset of samples in replicate on each system (values were the same to within analytical uncertainty). Previously we have checked results from both infrared spectroscopy-based systems in comparison to isotope ratio mass spectrometry for samples from the Madre de Dios system and found that these methods yielded comparable results (values the same within analytical uncertainty) [*Clark et al.*, 2014].

2.3.3. Solute Concentrations

The solute concentration data utilized in this study were previously published in *Torres et al.* [2016], and their methods are briefly reviewed here. Acidified samples were analyzed for cation (Na, K, Ca, Mg, Sr, and Li) as well as Si concentrations by microwave plasma atomic emission spectroscopy (Agilent 4100 MP-OES). Unacidified samples were analyzed for Cl^- and SO_4^{2-} concentrations by ion chromatography. Precision and accuracy were assessed by analyzing a reference material every 15 samples. For Cl, SO_4, Ca, Mg, Na, K, and Si, the reference material ION-915 was used (Environment Canada). For Li, the reference material TMDA-51.4 (Environment Canada) was used. For Sr, an in-house prepared $SrCO_3$ solution was used. Replicate analyses of each solution revealed an analytical precision within 5% (1σ) for each analyte.

2.4. Apportioning Solute Budgets of the Main Stem Madre de Dios

Our approach to apportion the water and solute fluxes between the four major tributaries of the Madre de Dios River is based on our new measurements of downstream changes in conservative tracers (data

Table 1. Wet Season Isotope and Solute Data

Sample	Date	δD	1σ	δ^{18}O	1σ	Cl (μM)	SO_4 (μM)	Na (μM)	Ca (μM)
Tributary-A	Mar 2013	−79.4	0.9	−11.8	0.1	3.5	95.7	83.7	119.2
Tributary-A (storm)	Mar 2013	−79.2	0.9	−11.7	0.1	3.1	68.4	77.1	94.2
Tributary-B	Mar 2013	−56.2	1.4	−8.6	0.02	3.3	70.0	149.2	722.2
Tributary-B (storm)	Mar 2013	−54.4	0.5	−8.4	0.1	3.5	72.4	144.2	743.8
Tributary-C	Mar 2013	−67.6	0.3	−10.2	0.2	1.7	10.5	55.3	14.6
Tributary-D	Mar 2013	−73.2	0.3	−10.7	0.3	1.6	11.1	53.8	54.8
Foreland-floodplain	Mar 2013	−70.3	0.4	−10.3	0.04	2.5	42.3	71.3	214.5
Upstream B	Mar 2013	−74.2	0.8	−11.1	0.1	3.5	88.0	89.5	174.4
Upstream B (storm)	Mar 2013	−81.2	0.9	−11.8	0.4	2.8	62.1	70.7	185.0
Downstream B	Mar 2013	−78.6	1.6	−11.5	0.1	2.9	64.8	78.4	244.8
Upstream C	Mar 2013	−73.9	1.6	−10.9	0.2	2.6	48.7	70.7	260.3
Downstream C	Mar 2013	−72.7	0.4	−10.5	0.1	2.5	40.3	68.1	183.3
Upstream D	Mar 2013	−72.8	1.1	−10.6	0.1	2.8	52.8	74.1	209.4
Downstream D	Mar 2013	−72.9	0.5	−10.8	0.05	2.4	44.4	71.9	181.5

reported in Tables 1 and 2). During field trips in March (wet season) and August (dry season) of 2013, samples were collected from each tributary as well as from the main stem upstream and downstream of each tributary confluence. Each confluence was sampled sequentially from upstream to downstream in the time span of a few days. At a confluence, samples were collected from the main stem and the tributary within the span of an hour. In May of 2016 (dry season), we resampled the confluence of tributaries A and B in order to verify the interannual consistency of the mixing ratio of these two tributaries, which dominate the budgets of most solutes (see below).

If there is a difference in the content of a conservative tracer (e.g., δD or Cl) between the main stem *upstream* of the confluence and the tributary, then a change in the conservative tracer measured in the main stem *downstream* of the confluence can be used to estimate the relative discharge of the tributary [*English et al*., 2000; *Bickle et al*., 2003; *Winston and Criss*, 2003]. This logic forms the basis of our approach to apportion water and solute fluxes between tributary subcatchments in the absence of gauging data for each tributary (see below). Our approach requires that the main stem and tributary are completely mixed when sampled downstream of the confluence. Consequently, we made sure to sample well downstream of each tributary confluence (approximately 4–12 km downstream) since mixing is known not to be instantaneous [e.g., *Bouchez et al*., 2010]. In supporting information Figures S2 and S3, we mark satellite images of each tributary confluence with the exact sampling localities.

2.4.1. Quantitative Tributary Mixing Model

At a tributary confluence, a change in a conservative tracer (e.g., δD or Cl) observed in the main stem after mixing reflects an addition of water. The total flow of the main stem can be partitioned into the relative amounts from the tributary and the main stem before mixing using the two end-member mixing equation:

Table 2. Dry Season Isotope and Solute Data

Sample	Date	δD	1σ	δ^{18}O	1σ	Cl (μM)	SO_4 (μM)	Na (μM)	Ca (μM)
Tributary-A	Aug 2013	−65.2	0.2	−10.4	0.1	11.7	163.1	121.1	190.3
Tributary-A (storm)	Aug 2013	−37.1	0.6	−7.2	0.2	8.6	71.6	81.7	108.4
Tributary-B	Aug 2013	−32.0	0.2	−6.6	0.1	8.6	117.8	199.6	715.0
Tributary-C	Aug 2013	−24.3	0.4	−5.3	0.5	4.6	31.9	85.7	84.8
Tributary-D	Aug 2013	−22.1	0.5	−5.0	0.4	2.6	11.4	64.4	50.5
Foreland-floodplain	Aug 2013	−25.2	0.3	−5.0	0.2	5.0	53.8	92.3	344.4
Upstream B	Aug 2013	−60.1	0.1	−9.8	0.02	15.3	164.5	124.0	319.8
Downstream B (storm)	Aug 2013	−31.9	0.2	−6.5	0.2	5.6	66.1	88.1	351.3
Downstream B	Aug 2013	−49.2	0.3	−8.1	0.7	11.0	143.8	119.1	336.5
Upstream C	Aug 2013	−39.3	0.4	−6.1	0.2				
Downstream C	Aug 2013	−37.6	0.3	−6.6	0.2				
Upstream D	Aug 2013	−37.1	0.3	−6.3	0.3				
Downstream D	Aug 2013	−29.9	0.3	−5.4	0.2				
Upstream B	May 2016	−41.1	1.1	−8.4	0.2				
Downstream B	May 2016	−43.8	1.2	−7.2	0.2				
Tributary-B	May 2016	−43.5	1.0	−6.4	0.2				

$$X_{river} = (F_{tributary} \times X_{tributary}) + (F_{upstream} \times X_{upstream}) \quad (1)$$

where X is the conservative tracer, F is the fraction of total discharge measured downstream of the confluence, subscript "tributary" refers to the adjoining tributary, and subscript "upstream" refers to the main stem upstream of the confluence. For a river system with multiple tributaries, a separate value of $F_{tributary}$ can be calculated for each tributary. In subsequent sections, the results from applying equation (1) will be termed mixing ratios.

If, in addition to the assumption of complete mixing, it is assumed (1) all the measured tributaries sum up to the total discharge of the river system, (2) the system is near a steady state with respect to discharge, and (3) that in-channel evaporation is negligible, then the individual $F_{tributary}$ values can be combined to determine the relative contribution of each tributary to the total discharge (Q_{total}). To do this, one can work "backwards" by first applying equation (1) to the most downstream tributary confluence (i.e., tributary-D). Since the discharge *upstream* of the tributary-D confluence should be the same as the discharge measured *downstream* of the tributary-C confluence, the calculated value of $F_{upstream}$ based on mixing at the tributary-D confluence can be used to link a preceding tributary (i.e., tributary-C) to the total discharge of the system. This approach can be summarized with the equation

$$Q_i = \begin{cases} F_i \times Q_{total} & i = J \\ F_i \times (Q_{total} - \sum_{s=i+1}^{J} Q_s) & i < J \end{cases} \quad (2)$$

where subscript i is the *ith* tributary (ordered downstream to upstream; i.e., D to A) and J is the total number of tributaries. In subsequent sections, the results from applying equation (2) will be termed mixing proportions.

3. Conservative Tracers in the Madre de Dios System

The ultimate goal of measuring changes in conservative tracers as the Madre de Dios River transits from its headwaters to our Foreland-floodplain sampling site is to quantify the relative contributions of each tributary to water and solute budgets (see section 4.1). With this in mind, we focus this section on the results that are most pertinent to the mixing model (equation (2)). This includes observations that will ultimately complicate the mixing model and add to the overall uncertainty of our analysis (e.g., section 3.1 below).

In Figure 3, we show the change in isotopic composition at each confluence for the March and August 2013 sampling campaigns. In general, each tributary has a distinct isotopic composition due to differences in catchment hypsometry (supporting information Figure S1) and the strong correlation between mean catchment elevation and the δD of river discharge (Figure 4). Seasonal and event-driven differences in the δD of each tributary were previously reported in *Ponton et al.* [2014]. Here, we also report seasonal and event-driven differences in the change in the isotopic composition of the main stem after each tributary confluence (Figure 3), which we will discuss extensively in subsequent sections.

3.1. Storm-Driven Variability in δD

During both the wet and dry seasons, storm events occurred while sampling near the confluence of tributaries A and B (Figure 2). Comparison between samples taken during storm and nonstorm conditions reveals some significant changes in δD values (Figure 3). For the purpose of deriving quantitative information about tributary mixing, of greatest importance are storm-driven variations in (1) the isotopic composition of the tributaries and (2) the isotopic difference between the main stem up and downstream of the confluence.

The only observed variation in the isotopic composition of a tributary during storm conditions was for tributary-A during the dry season, where the tributary δD is 28 ‰ higher during storm conditions ($\delta D = -37‰$) relative to nonstorm conditions ($\delta D = -65‰$). Potentially, this difference in δD results from a change in the source of runoff in response to increased precipitation [*Pearce et al.*, 1986; *Calmels et al.*, 2011; *Kirchner*, 2015]. During both the wet and dry seasons, storm-driven variations in the isotopic difference between the main stem up and downstream of the confluence of tributaries A and B were observed. In the wet season, there is no resolvable downstream change in the δD of the main stem during nonstorm conditions (change in $\delta D = 0.3 \pm 1.8‰$; 1σ propagated analytical uncertainty). In contrast, there is a downstream

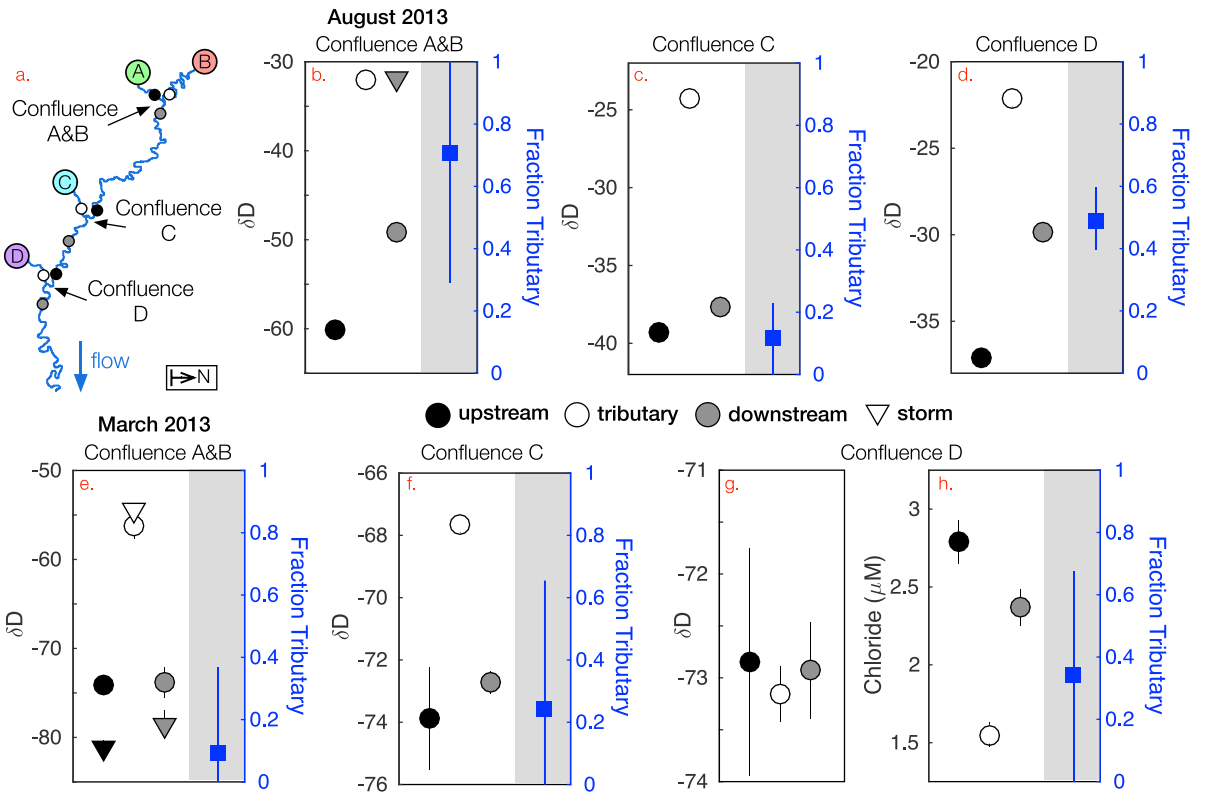

Figure 3. Conservative tracers at tributary confluences. For each confluence (i.e., A&B, C, and D; plot a), we show the δD(‰) of the main stem upstream of the confluence (black points), the tributary (white points), and the main stem downstream of the confluence (gray points). Nonstorm samples are shown as circles. Storm samples are shown as triangles. The dry season results (August 2013; plots b–d) are shown above the wet season results (March 2013; plots e–h). For confluence D during the wet season, we also show Cl concentrations (plot h) since δD values (plot g) are not sufficiently unique to allow a mixing ratio to be calculated. For each confluence, we also show the minimum, median, and maximum results of applying equation (1) to determine the proportion of the total discharge downstream of the confluence contributed by the tributary (blue squares). The locations of the sampling points on plot a are approximate. For the exact localities, see supporting information Figures S2 and S3.

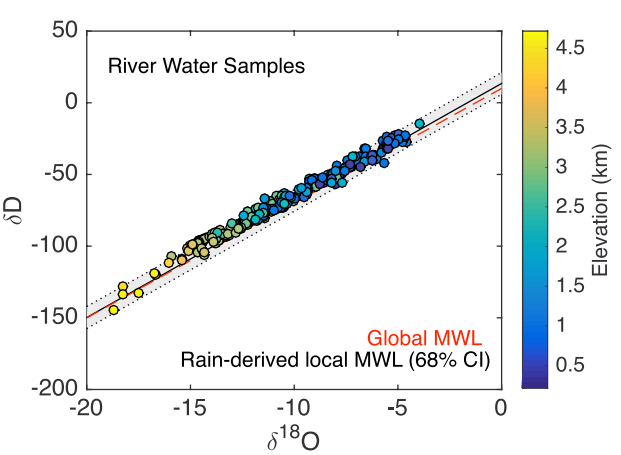

Figure 4. Local meteoric water line. The colored points show the water isotopic composition (in ‰) of rivers reported in this study as well as those of *Ponton et al.* [2014] and *Clark et al.* [2014]. The color of each point corresponds to its mean catchment elevation. The red-dashed line shows the global meteoric water line (MWL). The solid black line shows the local MWL defined by a linear regression of the precipitation samples of *Clark et al.* [2014] and *Feakins et al.* [2016]. The gray region around the local MWL bounded by dotted lines is the 68% confidence interval of the local MWL regression.

change in δD of 2.6 ± 1.8‰ during storm conditions in the wet season. In the dry season, the downstream change in δD is 10.9 ± 0.3 and 28.2 ± 0.2‰ for the nonstorm and storm conditions, respectively.

3.2. Downstream Evolution of Conservative Tracers

During both the wet and dry season sampling campaigns, we observed a downstream increase in the δD of river water (Figure 3). Importantly, the downstream increases in δD are accompanied by proportional changes in δ^{18}O such that all river waters within the study region (i.e., including the data from *Ponton et al.* [2014] and *Clark et al.* [2014]) plot along the same meteoric water line as defined by precipitation samples (Figure 4; precipitation data from *Clark et al.* [2014] and *Feakins et al.* [2016]), which implies

limited in-stream evaporation [*Craig et al.*, 1963].

During the 2013 wet season, the δD of the main stem after the confluence of tributaries A and B ($-73.9 \pm 1.6‰$) is $3.6 \pm 1.6‰$ lighter than the main stem at the most downstream sampling locality ($-70.3 \pm 0.4‰$; Figure 3a). A large portion ($2.6 \pm 0.6‰$) of the observed change occurs between the sampling locality downstream of the tributary-D confluence and the Foreland-floodplain site (Figure 3a). The remainder occurs at each of the tributary confluences (Figure 3). It is worth noting that the δD of tributary-D ($-73.2 \pm 0.3‰$) is not significantly different than the main stem upstream of the confluence ($-72.8 \pm 1.1‰$) during the wet season (Figure 3). That is to say, water isotopic ratios cannot be used to constrain the relative contribution of tributary-D during the 2013 wet season sampling. However, there is a significant difference in chloride concentrations between these two samples that can be used in lieu of δD in order to infer the relative contribution of tributary-D (1.6 ± 0.1 versus 2.8 ± 0.1 μM for tributary-D and the main stem, respectively). Downstream of the tributary-D confluence, the chloride concentration is significantly diluted (2.4 ± 0.1 μM) and does not change between downstream of the tributary-D confluence and the Foreland-floodplain site (Figure 3 and Table 1).

During the 2013 dry season, the δD of the main stem after the confluence of tributaries A and B ($-39.3 \pm 0.4‰$) is $14.2 \pm 0.5‰$ lighter than the main stem at the most downstream sampling locality ($-25.2 \pm 0.2‰$; Figure 3b). In contrast to the wet season, most of the observed downstream change in δD during the dry season occurs at tributary confluences, with the exception of a smaller ($4.7 \pm 0.4‰$) increase observed between the sampling locality downstream of the tributary-D confluence and the Foreland-floodplain site (Figure 3b). During both the August 2003 and May 2016 sampling campaigns (dry season), larger changes in water isotopic ratios are observed at the confluence of tributaries A and B than during the wet season (Figure 3; Tables 1 and 2).

4. Discussion

4.1. Application of the Tributary Mixing Model

Using the data reported in section 3, it is possible to apply equations (1) and (2) to solve for the mixing ratios at each confluence and the mixing proportions of each tributary. Here, we solve equation (1) using δD for all confluences except the tributary-D confluence in the dry season, where Cl concentrations are used because there is not a significant difference between the δD of the tributary and main stem upstream of the confluence (Figure 3). The minimum, maximum, and median results of these calculations (obtained via a Monte Carlo simulation of the analytical uncertainties; see supporting information MATLAB script) are reported for each confluence in Figure 3. For the confluences of tributaries A and B, where storm events affect tributary mixing ratios (section 3.1), we calculate separate mixing ratios for storm and nonstorm conditions using equation (1) and combine them to simulate the full range of possible mixing proportions using equation (2) (see supporting information MATLAB script).

As stated in section 2.4.1, many assumptions underlie the application of equation (2) to predict tributary mixing proportions. These include negligible in-stream evaporation, complete mixing, and quasi-steady state conditions with respect to discharge. Since all the water isotopic data plot along the local meteoric water line (Figure 4), it is likely that in-channel evaporation is negligible [*Craig et al.*, 1963]. However, it still remains unclear whether or not all of the assumptions required by equation (2) are met for each season. For example, we observed storm-driven variations in isotopic ratios at the confluence of tributaries A and B as well as variations in δD unrelated to major tributary inputs between tributary-D and the Foreland-floodplain station (Figure 3). Storm-driven variations in tributary mixing ratios (as indicated by changes in δD) may indicate nonsteady state behavior while changes in water isotopic ratios between confluences may suggest incomplete tributary mixing. An additional concern is whether or not the mixing proportions calculated using equation (1) changed significantly during the course of our sampling campaign ($\sim$3 days). Large changes in tributary mixing proportions between sampling times would invalidate our use of equation (2), which relies on combining data collected sequentially from each tributary.

To better constrain tributary mixing proportions during each sampling campaign given these uncertainties, we combine our inverse model (equation (2)) with a forward model that predicts Na and Cl concentrations of the main stem at the Foreland-floodplain site based on the calculated Q_i values (equation (2)) and measured Na and Cl concentrations of each tributary (Figure 5). Since each tributary has different Na and Cl

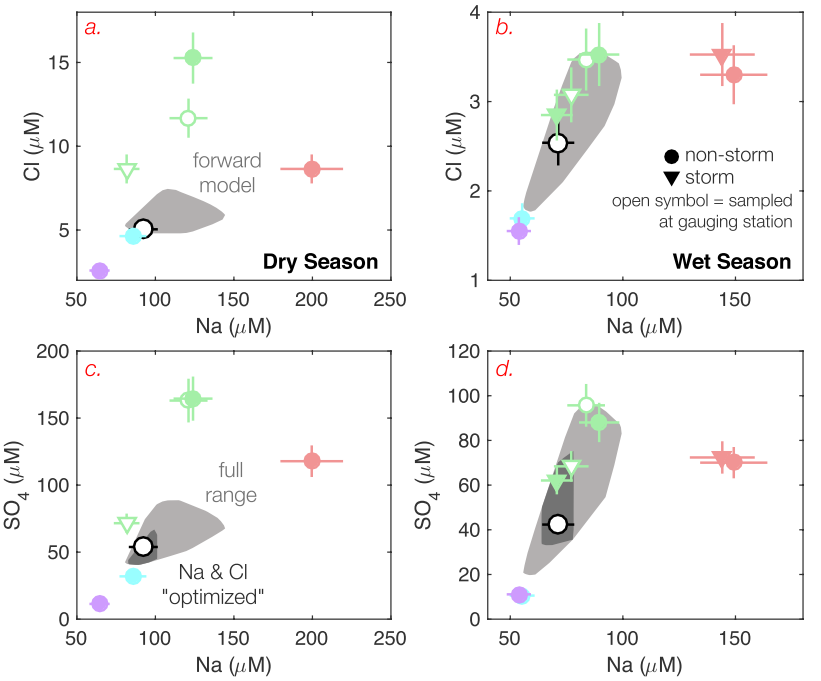

Figure 5. Mixing model-data comparison. The scatter plots compare the measured solute concentrations at the Foreland floodplain site (white circles) with those predicted by the mixing model (shaded gray area) using the measured solute concentrations of each tributary (colored points). For tributaries A and B, samples taken during storm and non-storm conditions are shown as triangles and circles respectively. For tributary A, samples collected at the gauging station of *Torres et al.* [2015] (and not upstream of the confluence with tributary B) are shown as open symbols. Na and Cl concentrations during the dry and wet seasons are shown in (a) and (b), respectively. Na and SO4 concentrations during the dry and wet seasons are shown in (c) and (d), respectively. In (c) and (d), the subset of mixing model results that agree with measured Na and Cl concentrations are shown with the darker shaded region. Measurements of tributaries A-D are shown as green, red, cyan, and purple symbols, respectively.

concentrations (Figure 5) and both Na and Cl are expected to mix conservatively [*Aucour et al.*, 2003; *Guinoiseau et al.*, 2016], the mixing proportions calculated from equation (2) should correctly predict the Na and Cl concentrations measured at the Foreland-floodplain station. To account for the analytical uncertainties and storm-driven variability in concentrations and isotopic ratios, we use a Monte-Carlo approach to sample 2000 random parameter combinations for each tributary mixing equation. Further model details are included within the supporting information MATLAB script. We note that for Tributary-A, we use contemporaneous solute concentrations measured more upstream of the confluence (at the Mountain-front gauging station of *Torres et al.* [2015] and *Torres et al.* [2016]), which, for the solutes considered here (Na, Cl, and SO_4) are comparable to concentrations measured directly at the confluence (Figure 5) and yield similar mixing model results.

In Figure 5, we show significant overlap between the measured and modeled Na and Cl concentrations, which suggests that the tributary mixing model provides reasonable estimates of the relative contributions of each of the four tributaries during both seasons. Superficially, the agreement between the measured and modeled values is better in the wet season relative to the dry season. We also note that the solute chemistry of tributaries C and D is sufficiently close that our model will be relatively insensitive to constraining their relative contributions beyond the results of equation (2). Instead, the model is most robust at distinguishing between the contributions of tributaries A, B, and C+D (Figure 5). For both seasons, our estimates of tributary discharge can be improved by finding the subset of mixing model results that reproduce Na and Cl concentrations within 5% of both measured values. Going forward, only these "optimized" model results will be used in the discussion.

The "optimized" model results can be used to predict the concentrations of all solutes measured for these samples (n = 23) [*Torres et al.*, 2015, 2016; *Baronas et al.*, 2017]. In principle, these additional solutes can also be used to further constrain the calculated mixing proportions. However, not all elements can serve as constraints on the mixing model results due to the potential for nonconservative mixing, which has previously

been identified for some elements (e.g., transition metals and rare earth elements) in the Amazon River system [*Aucour et al*., 2003; *Guinoiseau et al*., 2016]. Here, we discuss model results only for elements that are observed to mix conservatively (e.g., SO_4; Figure 5). The model results for elements that show nonconservative behavior (e.g., Mn, Fe, Co, Cd, and Nd) are discussed in a companion paper [*Baronas et al*., 2017]. We note that a majority of elements are calculated to mix conservatively in the Madre de Dios River (this study; *Baronas et al*., [2017]) and that the elements showing evidence for nonconservative mixing also display nonconservative behavior at other Amazonian confluences [*Aucour et al*., 2003; *Guinoiseau et al*., 2016].

4.2. Tributary Contributions to Discharge and Solute Fluxes

4.2.1. Inferences From the Mixing Model

If precipitation and rainfall-runoff relationships were spatially uniform across our catchment, the expectation is that the contribution of each tributary to total discharge would be equal to its catchment area. The results of our tributary mixing model imply heterogeneity in precipitation and/or rainfall-runoff relationships since the relative contribution of each tributary to the total discharge is not always equal to its catchment area (Figure 6). For example, the contribution of tributary-B is less than its catchment area during both the wet and dry seasons. Similarly, the contribution of tributary-D to discharge is greater than its catchment area during the dry season. While the relative contributions of each tributary to total discharge are highly uncertain, we note that the sum of all tributary contributions must be equal to one. For example, it is not possible for all of our estimates to simultaneously have their lowest predicted value since the results would not sum to one. While it not possible to display the covariation between different model results in a scatter plot, it is worth keeping this in mind when evaluating Figure 6.

In addition to spatial differences in the relative contributions of each tributary to total discharge, the results of our mixing model imply temporal variations as well. For example, estimates from the 2013 data set suggest that tributaries A and B contribute similar proportions of the total discharge in the dry season (Figure 6). However, in the wet season, the contribution of tributary-A is greater than that of tributary-B (Figure 6).

To test if the seasonal change in the mixing ratio of tributaries A and B is consistent year to year, we resampled the confluence of tributaries A and B in May 2016 (dry season). Consistent with our observations in August 2013, water isotopic ratios imply that the contributions of tributaries A and B are close to equal during the 2016 dry season (Figure 7). Since no rain events occurred during sampling in May 2016, the mixing results are more precise than those from the August 2013 data set and suggest that the contribution of tributary-B is in slight excess of tributary-A (Figure 7).

4.2.2. S Isotope Support for Inferred Variations in Tributary Mixing

Discharge-related variation in the mixing ratio of tributaries A and B could have important implications for C-Q relationships since the two catchments have distinct solute concentrations. To corroborate our inferences, we turn to additional evidence from S isotopes. Using the data reported in *Torres et al*.

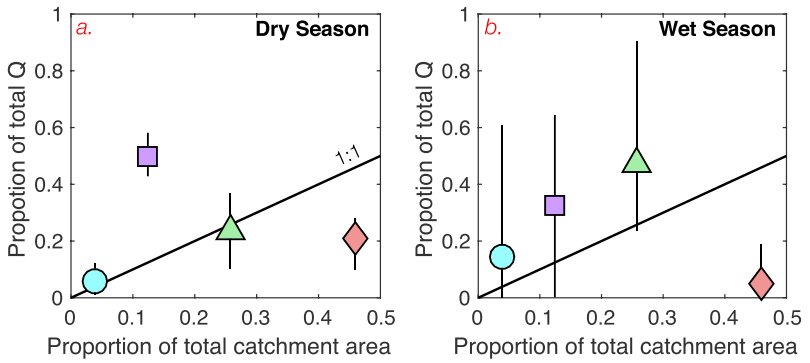

Figure 6. Relative contributions to total discharge. This scatter plot shows the proportion of total catchment area occupied by each tributary along with their predicted relative contribution to total discharge (Q). Panel a shows the results from the dry season sampling campaign (August 2013) while panel B shows the results from the wet season sampling campaign (March 2013). The location of each symbol is the median result while the error bars show the full range of model predictions. Note that the proportion of total Q sums to one for each model prediction. Consequently, not all combinations of mixing proportions defined by the ranges of each data point are possible (e.g., not all mixing proportions can simultaneously be at their lowest values). Results from tributaries A-D are shown as green triangles, red diamonds, cyan circles, and purple squares, respectively.

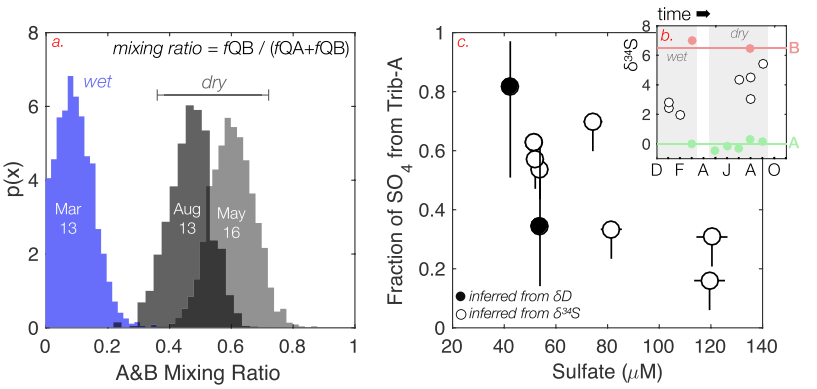

Figure 7. Evidence for seasonal variations in mixing ratios of tributaries A and B. (a) The probability density functions of calculated tributary mixing ratios at the confluence of tributaries A and B in March 2013 (blue), August 2013 (dark gray), and May 2016 (light gray). (b) δ^{34}S time-series collected at the Foreland-floodplain site (white points), tributary A (green points), and tributary B (red points). The solid lines show the average δ^{34}S values of tributaries A and B used for the mixing calculation presented in (c). The gray shading indicates the wet and dry seasons. In Figure 7c, the black points show the median and full range of measured SO_4 concentrations and the inferred proportions of the SO_4 flux contributed by tributary-A predicted using equation (2). The white points show the measured sulfate concentrations and the inferred proportions of the sulfate flux contributed by tributary-A predicted using the measured variations in sulfur isotopic ratios of dissolved sulfate at the Foreland-floodplain site. To determine this mixing proportion, we used a two-component mixing model with the δ^{34}S values of tributaries A and B equal to 0 and 6.5‰, respectively. Since this approach may overestimate the contribution of tributary-A (see section 4.2.2), we show asymmetric uncertainty bounds on these points.

[2016], we identify a large difference in the sulfur isotopic composition (δ^{34}S) of dissolved sulfate in tributaries A and B. Based on five samples, the δ^{34}S of tributary-A varies from -0.48 to $+0.29$‰ (analytical uncertainty $= \pm 0.2$‰) [*Torres et al.*, 2016]. Based on two samples, the δ^{34}S of tributary-B varies from $+6.4$ to $+6.9$‰.

Since the internal variability in δ^{34}S between the different samples from each tributary (~0.5‰) is much less than the difference between the two tributaries (6–7‰), variations in the mixing ratio of tributaries A and B will be robustly recorded in the δ^{34}S of the main stem at the Foreland-floodplain station. While tributaries C and D will also contribute to the sulfate and sulfur isotope budget of the main stem, their small contributions to total discharge (Figure 6) as well as their low sulfate concentrations (10–32 μM, versus 41–163 μM for tributaries A and B) mean that the sulfate flux of the main stem is dominated by the contributions of tributaries A and B. Indeed, the results of our tributary mixing model suggest that 83–97% and 78–89% of the sulfate flux at the Foreland-floodplain station is sourced from tributaries A and B during the wet and dry seasons, respectively. However, since tributaries C and D have similar δ^{34}S values to tributary A, treating the S isotope budget at the Foreland-floodplain site as a two-component mixing problem may overestimate the contribution of tributary-A and, as a result, should be considered a maximum estimate. We also note the sulfate concentrations at the Foreland-floodplain site predicted by the tributary mixing model match the observed concentrations during both seasons (i.e., sulfate mixes conservatively; Figure 5).

The δ^{34}S of the main stem at the Foreland-floodplain station ranges from $+1.9$ to $+5.5$‰ with minimum values during the wet season and maximum values during the dry season. These temporal variations in the δ^{34}S of the main stem are consistent with a greater contribution from tributary-A (lower δ^{34}S) relative to tributary-B (higher δ^{34}S) during the wet season (Figure 7). This is the same pattern predicted by water isotopic ratios using the tributary mixing model (Figure 6). Using a simple two-component mixing model (i.e., similar to equation (1)), δ^{34}S data imply the same mixing ratio of tributaries A and B as inferred from conservative tracers (Figure 7). In this way, the sulfur isotopic data corroborates our inference of a seasonal change in the relative contributions of tributaries A and B from downstream changes in δD and Cl concentrations.

4.3. Spatial and Temporal Variations in Precipitation

While there exists evidence for discharge-related variations in tributary mixing ratios (Figures 6 and 7), these observations do not alone constrain the origin of these variations. Potentially, tributary mixing ratios could vary in response to the spatiotemporal pattern of precipitation. For example, if seasonal variations in

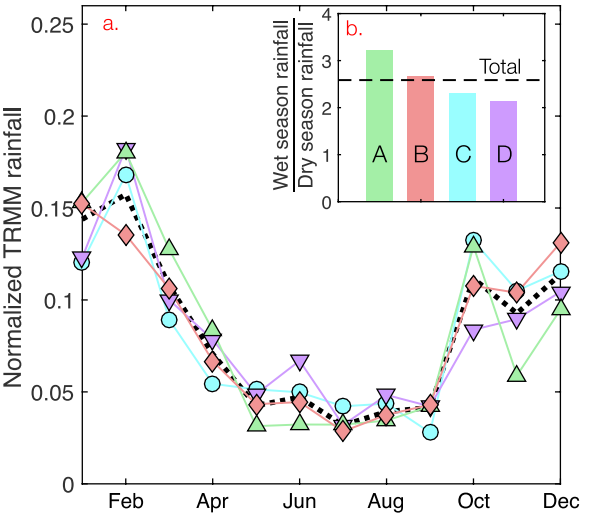

Figure 8. Spatiotemporal rainfall patterns from Tropical Rainfall Monitoring Mission (TRMM) precipitation estimates. (a) Average monthly 2B31 TRMM time-series (1998–2007) for each subcatchment in colored, solid lines with points. Time-series from tributaries A-D are shown as green triangles, red diamonds, cyan circles, and purple squares, respectively. The dashed black line without points refers to the total precipitation over the entire Foreland-floodplain catchment. For each 2B31 TRMM time-series, we normalized the monthly precipitation to the annual precipitation to investigate relative differences. (b) The ratio of wet (December-March) to dry (May-September) season precipitation for each sub-catchment determined by summing the monthly 2B31 TRMM time-series.

precipitation amounts were more extreme in one subcatchment relative to another, then the relative contributions of each tributary to total discharge could also vary seasonally (see example in Figure 1).

Previous studies have suggested that TRMM data do a poor job of capturing absolute precipitation amounts in the Andes Mountains [*Bookhagen and Strecker*, 2008; *Scheel et al*., 2010; *Espinoza et al*., 2015]. As a result, we limit our analysis to relative differences and focus on identifying the large-scale spatial and temporal patterns, which are thought to be captured accurately by TRMM data [*Bookhagen and Strecker*, 2008; *Scheel et al*., 2010; *Espinoza et al*., 2015]. In Figure 8, monthly TRMM precipitation amounts are normalized by the annual precipitation amount for each catchment.

Over the whole Foreland-floodplain catchment, precipitation amounts vary seasonally with a maximum during the wet season (December–March) and a minimum during the dry season (May–September; Figure 8a). The amplitude of this seasonal cycle varies spatially (Figure 8). Relative to the entire catchment, temporal variations in precipitation amounts are larger in the tributary-A catchment, lower in tributaries C and D, and approximately the same in the tributary-B catchment (Figure 8b).

Our analysis of 2B31 TRMM data suggests the amplitude of the seasonal cycle of precipitation is larger in the tributary-A catchment than the tributary-B catchment (Figure 8). As a result, the relative contribution of tributary-A to total precipitation increases during the wet season. This pattern is consistent with our inferences from sulfur isotopes and conservative tracers, which imply a greater contribution from tributary-A in the wet season (Figures 6 and 7). Thus, the spatiotemporal pattern of precipitation may be a key driver of variations in tributary mixing in this system.

4.4. Implications of Tributary Mixing for C-Q in the Madre de Dios System

As explained in the preceding sections 4.2 and 4.3, we observe seasonal variations in the mixing ratios of tributaries A and B (Figure 7) that may stem from differences in the seasonal pattern of precipitation in both catchments (Figures 8). Using sulfate as a representative solute, we find that 60–90% of the sulfate flux is sourced from tributary-A during the wet season (Figure 7). In contrast, during the dry season, only 20–30% of the sulfate flux is sourced from tributary-A (Figure 7). Whether these discharge-related variations in tributary mixing ratios affect the C-Q relationships observed at the Foreland-floodplain station depends on differences in the C-Q relationships of the individual tributary subcatchments.

Without additional measurements, it is difficult to robustly define the C-Q relationship of the tributary-B catchment. However, for some elements, differences in concentrations between tributaries A and B are so large that differences in C-Q relationships can be inferred from our limited data set. For example, during our 2013 sampling campaigns, Ca concentrations of Tributary-B were two (dry season) to four (wet season) times higher than the Ca concentrations of Tributary-A (sampled upstream of the confluence and *not* at the Mountain-front gauging station of *Torres et al*., [2015]). Thus, even if solute concentrations in both catchments were constant (i.e., "chemostatic"), seasonal changes in the mixing ratios of the two catchments would result in decreasing Ca concentrations with increasing discharge, as observed at the Foreland-floodplain station by *Torres et al*. [2015].

The fact that the dilution behavior observed at the Foreland-floodplain station by *Torres et al*. [2015] may stem, in part, from variations in tributary mixing ratios has important implications for how C-Q relationships are interpreted in this system. While the preferred interpretation of *Torres et al*. [2015] linked C-Q relationships to the combined effects of erosion and hydrology on chemical weathering, they acknowledged tributary mixing as a potential driver. The results of the present study suggest that variations in tributary mixing ratios significantly modulate C-Q relationships such that any underlying relationships between erosion, hydrology, and weathering may be obscured. Thus, in order to identify if these relationships exist in the Madre de Dios system, it is necessary to account for the observed variations in tributary mixing.

For the two sampling periods where we can apportion water and solute budgets between each of the four tributaries, it is possible to investigate whether solute generation varies systematically with the proportion of Andean catchment area, as implied by *Torres et al*. [2015]. To do this, we normalize the relative contribution of each tributary to the flux of a solute (f_C) by its contribution to total discharge (f_Q). Essentially, this normalization just compares the solute concentrations of each catchment, but in a manner that scales these differences to the solute flux of the entire system.

If the solute concentrations of each tributary were identical, then the contribution of each tributary to solutes fluxes would be equal to its contribution to total discharge ($f_C/f_Q = 1$). When f_C/f_Q for a tributary is greater than one, the tributary contributes disproportionately to solute fluxes due to high solute concentrations. If f_C/f_Q for a tributary is less than one, the tributary contributes more to discharge than solute fluxes due to low solute concentrations.

In the Madre de Dios system, tributaries with low proportions of Andean catchment area (Tributaries C and D) have ratios of f_C to f_Q that are less than one for Na and SO_4 (Figure 9). In contrast, tributaries with a greater proportion of Andean catchment area (Tributaries A and B) have ratios of f_C to f_Q that are greater than or equal to one for Na and SO_4 (Figure 9).

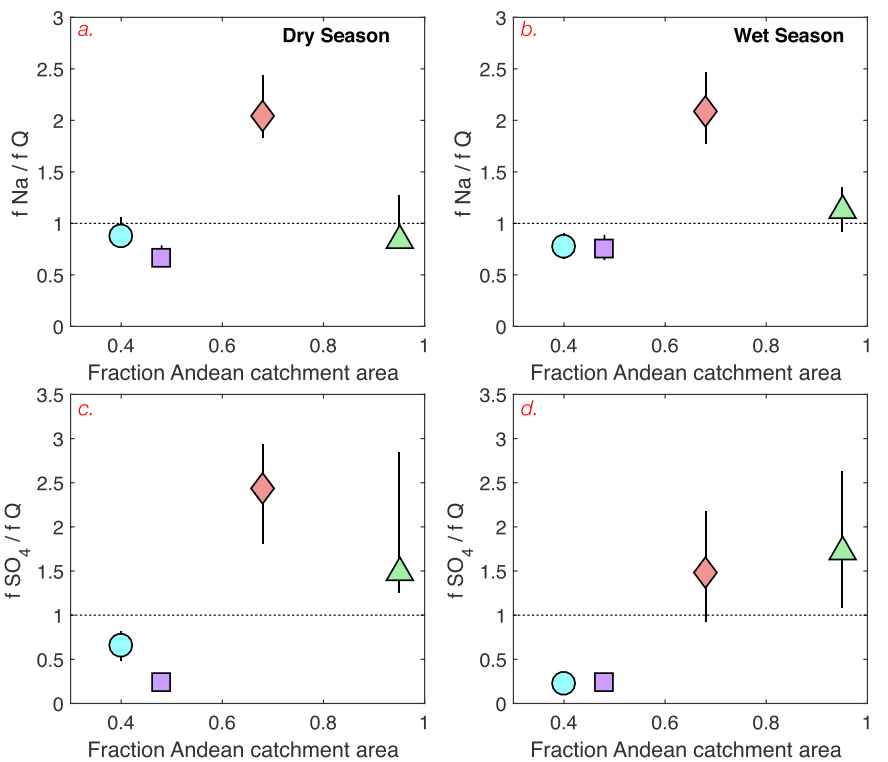

Figure 9. Variations in tributary contributions to solute fluxes. On the *y* axis of plots a and b, we show the proportion of the Na flux (*f*Na) contributed by each tributary normalized by their relative contributions to discharge (*f*Q). The *y* axis in plots c and d shows this same metric, but for SO_4 fluxes. All *x* axes show the portion of the catchment area greater than 400 m in elevation (i.e., Andean area). Results obtained during the dry and wet seasons are shown on the left and right plots, respectively. All points are located at the median value of the model results with the error bar showing the full range of model predictions. Results from tributaries A-D are shown as green triangles, red diamonds, cyan circles, and purple squares, respectively.

These results suggest that solute generation is more "efficient" in Andean portions of the catchment relative to lower elevations. For example, both tributaries A and D contribute similar proportions of total discharge, but, for this same water flux, tributary-A generates significantly higher solute concentrations (Figure 9). Thus, while C-Q relationships at the Foreland-floodplain station may be modulated by tributary mixing, an underlying link between erosion, hydrology, and chemical weathering may still exist in the Madre de Dios system. We note that our observation of a disproportionate contribution of Andean tributaries to solute fluxes is in line with numerous previous studies of the Andes/Amazon system [*Gibbs*, 1967; *Stallard and Edmond*, 1983; *Gaillardet et al*., 1997; *Moquet et al*., 2011].

5. Wider Implications: When and Why Is Mixing Expected to Modulate C-Q Relationships?

The effects of tributary mixing on C-Q relationships should depend on both (1) the variability in tributary mixing ratios and (2) differences in C-Q relationships for each of the constituent tributaries. Consequently, it is possible for different solutes to respond differently to the same changes in tributary mixing ratios. As a result, identifying variations in tributary mixing ratios alone does not mean that the observed C-Q patterns are affected by this mixing.

To explore the range of effects that can be caused by tributary mixing more generally, we take two distinct approaches. First, we develop a simple two tributary mixing model to investigate the effects of different tributary C-Q relationships and runoff time-series on the C-Q behavior of the aggregate catchment (Figure 10). Second, to explore differing responses of different elements within the same system, as predicted in the model, we reanalyze data from *Torres et al*. [2015] that were collected in a nested pair of Andean headwater catchments (Figure 11a; Mountain-1 (upper) and Mountain-2 (total) catchments of *Torres et al*. [2016]). By dividing the total catchment into upper and lower (total minus upper) portions, we can compare the C-Q relationships of the two constituent tributaries (upper and lower) to the C-Q relationships of the aggregate river (i.e., analogous to our model setup).

5.1. Two Tributary Mixing Model

To predict the possible effects of tributary mixing on C-Q relationships, we start by considering two tributaries (T1 and T2) that mix conservatively and completely to form an aggregate river (R). Both tributaries are assumed to have power law C-Q relationships ($C = aQ^b$) with different values of the multiplicative prefactor (a) and exponent (b). Similarly, the runoff time-series of each tributary are assumed to be sinusoidal functions of time ($Q = A \times \sin(2\pi ft - \varphi) + k$) with different amplitudes (A) and phase-lags (φ), but the same frequency (f) and mean values (k). At any given time, the discharge of the aggregate river is equal to the sum of the two rivers while the concentration is the discharge-weighted average of the two tributaries (i.e., equation (1)). Though a simplification of real catchment hydrology and hydrochemistry, this model setup allows us to explore basic system behavior.

Despite its simplicity, our two tributary mixing model contains four distinct parameters (a, b, A, and φ) making it difficult to succinctly show all possible model behaviors. In lieu of an exhaustive exploration of parameter space, we show a few representative examples that are relevant to interpreting the C-Q behaviors of rivers with heterogeneous catchment areas. In Figure 10a, we show how variations in tributary mixing ratios only minimally impact the C-Q behavior of the aggregate catchment if the two tributaries have very similar C-Q relationships. In Figure 10b, we show how variations in tributary mixing in concert with differences in the multiplicative prefactor (a) can result in a b-exponent of the aggregate river that is distinct from either of its constituent subcatchments. Similarly, in Figure 10c, we show an example of how mixing between tributaries with different b-exponents affects the b-exponent of the aggregate river. Finally, in Figure 10d, we show an example where differences in the C-Q relationships and phase-lag of the runoff time-series of each tributary lead to significant hysteresis in the C-Q relationship of the aggregate river. We note that previous work on the largest tributaries of the Amazon River by *Moquet et al*. [2015] attributed the observed hysteresis in the C-Q relationship of the main stem to differences in C-Q relationships and runoff phase-lags between its constituent tributaries (i.e., analogous to the model results shown in Figure 10d).

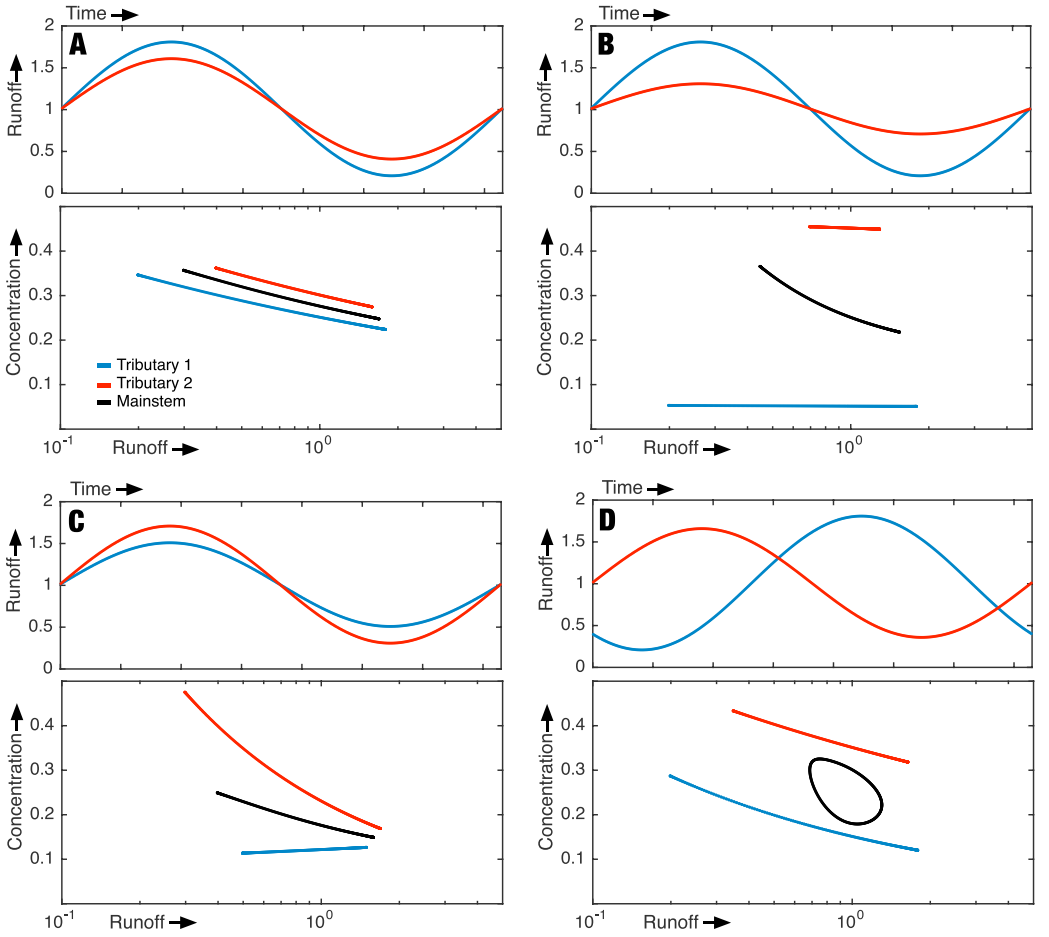

Figure 10. Modeled theoretical tributary mixing relationships. (a–d; top) The runoff time-series and (bottom) C-Q relationships for two tributaries (1 and 2) that combine to form the main stem. In Figure 10a, model parameters are selected to produce a C-Q relationship of the main stem that deviates little from its constituent tributaries (A1 = 0.8, A2 = 0.6, a1 = 0.25, a2 = 0.3, b1 = −0.2, b2 = −0.2, φ=0). Figures 10b and 10c show model results where the C-Q relationship of the main stem are substantially different than the constituent tributaries due to contrasting multiplicative pre-factors (b; A1 = 0.8, A2 = 0.3, a1 = 0.05, a2 = 0.45, b1 = −0.02, b2 = −0.02, φ=0) and power law exponent (c; A1 = 0.5, A2 = 0.7, a1 = 0.12, a2 = 0.23, b1 = 0.1, b2 = −0.6, φ=0). In Figure 10d, model parameters are selected to produce C-Q hysteresis (A1 = 0.8, A2 = 0.65, a1 = 0.15, a2 = 0.35, b1 = −0.4, b2 = −0.2, φ=4).

5.2. Field Data From the Andean Kosñipata River

The examples shown in Figure 10 highlight that variations in tributary mixing ratios can have a variety of effects on the observed C-Q behavior including none (Figure 10a), modulated b values (Figures 10b and 10c), and hysteresis (Figure 10d). Since C-Q relationships are not the same for every solute within a single catchment [*Godsey et al*., 2009; *Moon et al*., 2014; *Stallard and Murphy*, 2014; *Torres et al*., 2015], each solute may respond differently to imposed variations in tributary mixing ratios at a single site. With this potential for solute-to-solute variability in mind, we reanalyze solute concentration [*Torres et al*., 2015] and discharge [*Clark et al*., 2014] data from the Andean Kosñipata River catchment to explore how the b-exponent of the C-Q relationships for different solutes is affected by variations in tributary mixing ratios.

In Figure 11a, we show a map of the Andean Kosñipata River and mark the two gauging stations used in this study, referred to here as "upper" (reflecting the catchment area at the Wayqecha station) and "total" (reflecting the catchment area at the San Pedro station). We divide the total catchment area of Kosñipata River at the San Pedro gauging station (total; 161 km^2) into an upper portion (upper; 50 km^2) and a lower portion (total minus upper; 111 km^2; Figure 11a). Simultaneous measurements of solute concentrations and discharge from the upper portion and the total catchment allow for the concentrations and discharge of the lower portion to be determined by difference. We can then compare the C-Q relationships of the upper

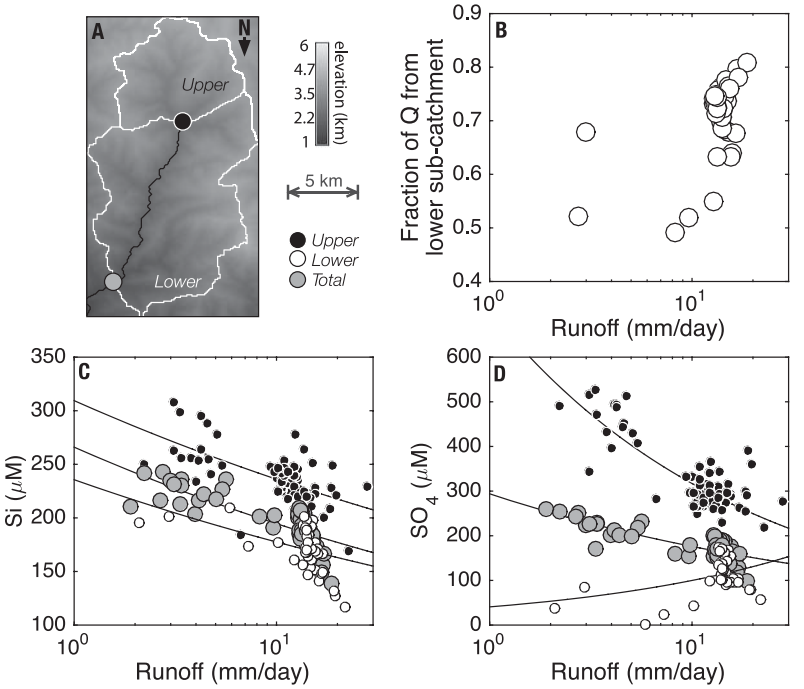

Figure 11. Effects of tributary mixing in a small Andean catchment. (a) Map of the Kosñipata River catchment sampled by *Torres et al.* [2015] between September 2010 and February 2011 (for location, see Figure 2). (b) The proportions of total discharge supplied by the lower subcatchment determined by gauging the upper portion and the total catchment simultaneously. (c) The relationship between dissolved Si and runoff for the upper portion, lower portion, and total catchment. (d) The relationship between dissolved SO_4 and runoff for the upper portion, lower portion, and total catchment. Note that the *x* axes in each scatter plot have logarithmic scaling.

(observed) and lower (calculated) portions of the catchment with the C-Q relationship of the total catchment (observed; Figures 11c and 11d).

We find significant variations in the mixing ratios of the upper and lower portions of the catchment (Figure 11b). Generally, the relative contribution of the lower portion of the catchment to total discharge is higher at high discharge, but there is considerable scatter in this relationship (Figure 11b). For Si, the observed variations in the relative contributions of water from the upper and lower portions do not appear to affect C-Q relationships of the total catchment (Figure 11c). If the variation in Si with runoff (R) is modeled as a single power law relationship ($Si \propto R^b$), the calculated power law exponent (b) is not significantly different between the upper portion, lower portion, and total catchment area (Figure 11c). In other words, we see little effect of tributary mixing on the aggregate C-Q relationship. Consistent with the model results shown in Figure 10a, the lack of a tributary mixing effect for Si results from the fact that both tributary subcatchments have nearly identical Si-Q relationships (Figure 11c).

In contrast to Si, variations in tributary mixing ratios appear to significantly modulate the observed C-Q relationship for SO_4 in the total Kosñipata catchment (Figure 11d). A power law model for the relationships between SO_4 and runoff yields distinct b-exponents for the upper and lower portion of the catchment, with the total catchment having a distinct intermediate b-exponent (Figure 11d). This result is analogous to the model results presented in Figures 10c and 10d, where differences in the C-Q behavior of the tributaries leads to an aggregate behavior that is distinct relative to the two constituent subcatchments (Figure 11d).

Likely, the contrasting behavior of Si versus SO_4 in this system stems from the observed spatial variations in lithology. The upper proportion of the Andean Kosñipata River catchment is underlain by sulfur-rich metasedimentary rocks while the lower portion contains both metasediments and sulfur-poor granitic rocks [*Torres et al.*, 2016]. While at a different scale than the entire Madre de Dios system (160 km^2 versus 28×10^3 km^2), this analysis of tributary mixing in the Andean Kosñipata River is consistent with our simplified model of theoretical mixing behavior (Figure 10) and provides a useful example of how tributary mixing

may affect certain solutes to a greater extent than others depending on spatial variations in C-Q relationships. This element specificity is explored in more detail in our companion paper [*Baronas et al.,* 2017].

6. Conclusions

Using water isotopes, chloride, and sodium as conservative tracers, we apportioned the water and solute budgets of the Madre de Dios River between its four major tributaries during two sampling campaigns, in the wet and dry seasons, respectively. Our results suggest that relative contributions of the two dominantly Andean tributaries vary systematically with discharge due to the observed spatiotemporal pattern of precipitation. The implied pattern of tributary mixing matches variations in the sulfur isotopic ratios of dissolved sulfate measured at a wider range of discharge conditions [*Torres et al*., 2016], which suggests that our predictions from the detailed sampling campaigns capture the annual pattern of tributary mixing.

Due to their distinct solute concentrations, the observed pattern of mixing between the two Andean tributaries matches our previous observations of dilution within increasing discharge for the main stem river, particularly for Ca [*Torres et al*., 2015]. Based on our simplified two tributary mixing model, we expect the relative importance of tributary mixing in setting C-Q relationships to be element specific, which we explore in more detail in a companion paper [*Baronas et al*., 2017]. While we find evidence for modulation of the C-Q relationship by tributary mixing, accounting for this behavior substantiates the idea of an underlying link between erosion, hydrology, and weathering in the Madre de Dios system as suggested by *Torres et al*. [2015].

Beyond the data reported in this study, previous work has highlighted a key role for tributary mixing in driving variations in the solute chemistry of large rivers. For example, in a study of the Fraser River system, *Voss et al*. [2014] linked temporal variability in the strontium isotopic composition of the main stem to variations in the relative contributions of tributary subcatchments draining different lithologies. Similarly, *Moquet et al*. [2015] linked the hysteresis in C-Q behavior of the Amazon River at its mouth to variations in the relative contributions of its major tributaries. Taken all together, this and other work suggests that the dynamics of solute concentrations in large, heterogeneous catchments stems not only from hillslope processes [*Godsey et al*., 2009; *Maher*, 2011; *Maher and Chamberlain*, 2014], but also from variations in tributary mixing ratios. As a result, independent constraints on the effects of tributary mixing are required in order to accurately interpret C-Q relationships in heterogeneous catchment systems.

Acknowledgments
Financial support was provided by NSF EAR-1227192 and NSF EAR-1455352. M. Torres was supported by USC and C-DEBI fellowships. We thank ACCA Peru, Incaterra, and CREES for field support. We thank Camilo Ponton, Valier Galy, Adan Ccahuana, Emily Burt, and the 2016 USC Field Geology class for field assistance. Zhenyu (David) Fu is thanked for drafting supporting information Figures S1 and S2. All the data utilized in this study are available either in Tables 1 and 2 or in the original publications [*Clark et al*., 2014; *Torres et al*., 2015, 2016].

References

Anderson, S. P., W. E. Dietrich, R. Torres, D. R. Montgomery, and K. Loague (1997), Concentration-discharge relationships in runoff from a steep, unchanneled catchment, *Water Resour. Res.*, *33*(1), 211–225, doi:10.1029/96WR02715.

Aucour, A.-M., F.-X. Tao, P. Moreira-Turcq, P. Seyler, S. Sheppard, and M. Benedetti (2003), The amazon river: Behaviour of metals (fe, al, mn) and dissolved organic matter in the initial mixing at the rio negro/solimes confluence, *Chem. Geol.*, *197*(14), 271–285, doi:10.1016/S0009-2541(02)00398-4.

Baronas, J. J., M. A. Torres, K. E. Clark, and A. J. West (2017), Mixing as a driver of temporal variations in river hydrochemistry: 2. Major and trace element concentration dynamics in the Andes-Amazon transition, *Water Resour. Res.*, *53*, doi:10.1002/2016WR019729.

Bickle, M., J. Bunbury, H. Chapman, N. Harris, I. Fairchild, and T. Ahmad (2003), Fluxes of Sr into the headwaters of the Ganges, *Geochim. Cosmochim. Acta*, *67*(14), 2567–2584, doi:10.1016/S0016-7037(03)00029-2.

Bookhagen, B., and M. R. Strecker (2008), Orographic barriers, high-resolution TRMM rainfall, and relief variations along the eastern Andes, *Geophys. Res. Lett.*, *35*, L06403, doi:10.1029/2007GL032011.

Bouchez, J., E. Lajeunesse, J. Gaillardet, C. France-Lanord, P. Dutra-Maia, and L. Maurice (2010), Turbulent mixing in the Amazon River: The isotopic memory of confluences, *Earth Planet. Sci. Lett.*, *290*(1–2), 37–43, doi:10.1016/j.epsl.2009.11.054.

Calmels, D., A. Galy, N. Hovius, M. Bickle, A. J. West, M.-C. Chen, and H. Chapman (2011), Contribution of deep groundwater to the weathering budget in a rapidly eroding mountain belt, Taiwan, *Earth Planet. Sci. Lett.*, *303*(1–2), 48–58, doi:10.1016/j.epsl.2010.12.032.

Carlotto Caillaux, V. S., G. Rodriguez, W. Fernando, C. Roque, J. Dionicio, and R. Chávez (1996), Geología de los cuadrángulos de Urubamba y Calca, *Tech. Rep. 65*, Inst. Geol. Nac., Lima, Peru.

Clark, K. E., et al. (2014), The hydrological regime of a forested tropical Andean catchment, *Hydrol. Earth Syst. Sci.*, *18*(12), 5377–5397, doi:10.5194/hess-18-5377-2014.

Craig, H., L. I. Gordon, and Y. Horibe (1963), Isotopic exchange effects in the evaporation of water, *J. Geophys. Res.*, *68*(17), 5079–5087.

English, N. B., J. Quade, P. G. DeCelles, and C. N. Garzione (2000), Geologic control of Sr and major element chemistry in Himalayan Rivers, Nepal, *Geochim. Cosmochim. Acta*, *64*(15), 2549–2566, doi:10.1016/S0016-7037(00)00379-3.

Espinoza, J. C., S. Chavez, J. Ronchali, C. Junquas, K. Takahashi, and W. Lavado (2015), Rainfall hotspots over the southern tropical Andes: Spatial distribution, rainfall intensity, and relations with large-scale atmospheric circulation, *Water Resour. Res.*, *51*, 3459–3475, doi:10.1002/2014WR016273.

Feakins, S. J., et al. (2016), Plant leaf wax biomarkers capture gradients in hydrogen isotopes of precipitation from the Andes and Amazon, *Geochim. Cosmochim. Acta*, *182*, 155–172.

Gaillardet, J., B. Dupre, C. Allegre, and P. Négrel (1997), Chemical and physical denudation in the Amazon River Basin, *Chem. Geol.*, *142*(3–4), 141–173.
Gaillardet, J., B. Dupré, P. Louvat, and C. J. Allegre (1999), Global silicate weathering and CO2 consumption rates deduced from the chemistry of large rivers, *Chem. Geol.*, *159*(1–4), 3–30.
Gibbs, R. (1967), The geochemistry of the Amazon river system: Part I. The factors that control the salinity and the composition and concentration of the suspended solids, *Geol. Soc. Am. Bull.*, *78*, 1203–1232.
Godsey, S., J. Kirchner, and D. Clow (2009), Concentration discharge relationships reflect chemostatic characteristics of US catchments, *Hydrol. Processes*, *1864*, 1844–1864, doi:10.1002/hyp.7315.
Guinoiseau, D., J. Bouchez, A. G. Elabert, P. Louvat, N. Filizola, and M. F. Benedetti (2016), The geochemical filter of large river confluences, *Chem. Geol.*, *441*, 191–203, doi:10.1016/j.chemgeo.2016.08.009.
Herndon, E. M., A. L. Dere, P. L. Sullivan, D. Norris, B. Reynolds, and S. L. Brantley (2015), Landscape heterogeneity drives contrasting concentration discharge relationships in shale headwater catchments, *Hydrol. Earth Syst. Sci.*, *19*(8), 3333–3347, doi:10.5194/hess-19-3333-2015.
Ibarra, D. E., J. K. Caves, S. Moon, D. L. Thomas, J. Hartmann, C. P. Chamberlain, and K. Maher (2016), Differential weathering of basaltic and granitic catchments from concentration-discharge relationships, *Geochim. Cosmochim. Acta*, *190*, 265–293.
INGEMMET (2013), GEOCATMIN: Geologia integrada por proyectos regionales, technical report, Inst. Geol. Min. Metal., Instituto Geológico, Minero, y Metalúrgico.
Jarvis, A., H. I. Reuter, A. Nelson, and E. Guevara (2008), *Hole-Filled SRTM for the Globe Version 4*. [Available at CGIAR-CSI SRTM 90m Database, http://srtm.csi.cgiar.org.]
Johnson, N., G. Likens, F. Bormann, D. Fisher, and R. Pierce (1969), A working model for the variation in stream water chemistry at the Hubbard brook experimental forest, New Hampshire, *Water Resour. Res.*, *5*(6), 1353–1363.
Kim, H., J. K. Bishop, W. E. Dietrich, and I. Y. Fung (2014), Process dominance shift in solute chemistry as revealed by long-term high-frequency water chemistry observations of groundwater flowing through weathered argillite underlying a steep forested hillslope, *Geochim. Cosmochim. Acta*, *140*, 1–19, doi:10.1016/j.gca.2014.05.011.
Kirchner, J. W. (2015), Aggregation in environmental systems: Catchment mean transit times and young water fractions under hydrologic nonstationarity, *Hydrol. Earth Syst. Sci.*, *12*, 3105–3167, doi:10.5194/hessd-12-3105-2015.
Lambs, L., A. Horwath, T. Otto, F. Julien, and P.-O. Antoine (2012), Isotopic values of the Amazon headwaters in Peru: Comparison of the wet upper Río Madre de Dios watershed with the dry Urubamba-Apurimac river system., *Rapid Commun. Mass Spectrom.*, *26*(7), 775–84, doi:10.1002/rcm.6157.
Maher, K. (2011), The role of fluid residence time and topographic scales in determining chemical fluxes from landscapes, *Earth Planet. Sci. Lett.*, *312*(1–2), 48–58, doi:10.1016/j.epsl.2011.09.040.
Maher, K., and C. P. Chamberlain (2014), Hydrologic regulation of chemical weathering and the geologic carbon cycle, *Science*, 1502–1504, doi:10.1126/science.1250770.
Mendívil Echevarría, S., and D. Dávila Manrique (1994), Geología de los cuadrángulos de Cuzco y Livitaca, *Tech. Rep. 54*, Inst. Geol. Nac., Lima, Peru.
Moon, S., C. Chamberlain, and G. Hilley (2014), New estimates of silicate weathering rates and their uncertainties in global rivers, *Geochim. Cosmochim. Acta*, *134*, 257–274, doi:10.1016/j.gca.2014.02.033.
Moquet, J.-S., et al. (2011), Chemical weathering and atmospheric/soil CO2 uptake in the Andean and Foreland Amazon basins, *Chem. Geol.*, *287*(1–2), 1–26, doi:10.1016/j.chemgeo.2011.01.005.
Moquet, J.-S., et al. (2015), Amazon River dissolved load: Temporal dynamics and annual budget from the Andes to the ocean, *Environ. Sci. Pollut. Res.*, *23*, 1–25, doi:10.1007/s11356-015-5503-6.
Pearce, A., M. Stewart, and M. Sklash (1986), Storm runoff generation in humid headwater catchments: 1. Where does the water come from?, *Water Resour. Res.*, *22*(8), 1263–1272.
Ponton, C., A. J. West, S. J. Feakins, and V. Galy (2014), Leaf wax biomarkers in transit record river catchment composition, *Geophys. Res. Lett.*, *41*, 6420–6427, doi:10.1002/2014GL061328.
Scheel, M. L. M., M. Rohrer, C. Huggel, D. Santos Villar, E. Silvestre, and G. J. Huffman (2010), Evaluation of TRMM Multi-satellite Precipitation Analysis (TMPA) performance in the Central Andes region and its dependency on spatial and temporal resolution, *Hydrol. Earth Syst. Sci. Discuss.*, *7*(5), 8545–8586, doi:10.5194/hessd-7-8545-2010.
Stallard, R. F., and J. M. Edmond (1983), Geochemistry of the Amazon 2. The influence of geology and weathering environment on the dissolved load, *J. Geophys. Res.*, *88*(C14), 9671–9688.
Stallard, R. F., and S. F. Murphy (2014), A unified assessment of hydrologic and biogeochemical responses in research watersheds in eastern Puerto Rico using runoff–concentration relations, *Aquat. Geochem.*, *20*(2–3), 115–139.
Torres, M. A., A. J. West, and K. E. Clark (2015), Geomorphic regime modulates hydrologic control of chemical weathering in the Andes-Amazon, *Geochim. Cosmochim. Acta*, *166*, 105–128, doi:10.1016/j.gca.2015.06.007.
Torres, M. A., A. J. West, K. E. Clark, G. Paris, J. Bouchez, C. Ponton, S. J. Feakins, V. Galy, and J. F. Adkins (2016), The acid and alkalinity budgets of weathering in the Andes Amazon system: Insights into the erosional control of global biogeochemical cycles, *Earth Planet. Sci. Lett.*, *450*, 381–391, doi:10.1016/j.epsl.2016.06.012.
Vargas Vilchez, L., and A. Hipolito Romero (1998), Geología de los cuadrángulos de Río Pinquén, Pilcopata y Chontachaca. Hojas: 25-t, 26-t y 27-t, *Tech. Rep. 116*, Inst. Geol. Nac., Lima, Peru.
Voss, B. M., et al. (2014), Tracing river chemistry in space and time: Dissolved inorganic constituents of the Fraser River, Canada, *Geochim. Cosmochim. Acta*, *124*, 283–308, doi:10.1016/j.gca.2013.09.006.
Winston, W., and R. Criss (2003), Oxygen isotope and geochemical variations in the Missouri river, *Environ. Geol.*, *43*(5), 546–556.